Transient thermal behaviour of a solid oxide fuel cell

Moussa Chnani, Marie-Cécile Péra, Raynal Glises, J.M. Kauffmann, Daniel Hissel

Transient thermal behaviour of a solid oxide fuel cell

Moussa Chnani, Marie-Cécile Péra, Raynal Glises, Jean Marie Kauffmann and Daniel Hissel

University of Franche-Comte

University of technology of Belfort-Montbeliard

Laboratory of Electrical Engineering and Systems (L2ES)

Tel: + 3 33 84 58 36 25

e-Mail : moussa.chnani@utbm.fr

Abstract

A macroscopic model of a short SOFC stack has been developed. The first part of this paper intends to describe a methodology for determining the transient thermal behaviour of the SOFC. A nodal network is used in order to determine the final internal temperatures of the structure. The stack is modelled by one average cell. The cell is divided into several isothermal volumes represented by their central node. The energy balances at each node are developed and solved by Matlab routine. The second part describes a fluidic model in order to compute the partial pressures of chemical species and the output flows. The fluidic model uses electrical/fluidic analogy. Pressure drops in channels are modelled through resistances and the fluid accumulation in the volume is modelled by a capacitor. The next part describes the electrochemical model based on the classical Nernst equation and computation of the overpotential (activation, concentration and ohmic overvoltage). The three submodels are then coupled in order to built a complete modelling of the stack. It has been validated and compared with experimental results on an SOFC stack provided by HTceramix.

Keywords: Solid oxide fuel cell; Transient thermal modelling; Fluidic and Electrochemical modelling.

1- Introduction

The solid oxide fuel cell (SOFC) is a promising technology. It is highly efficient, tolerant to impurities so it is fuel flexible (methane or even gasoline and diesel), and it can provide internal reforming of hydrocarbon fuels, at least partially. The work presented in this paper is in the frame work of the European project FELICITAS, FP 6, which aims to increase efficiency and life time of FC systems for heavy duty transportation applications (marine, rail, truck). One of the topics is the study of the hybridization of a PEFC and a SOFC. The model proposed here addresses a macroscopic simulation of a SOFC stack. It aims to be included in

the simulation of the SOFC and PEFC coupling.

The SOFC modeling is an essential tool as fuel cell behaviour is driven by several coupled phenomena: fuel and oxidant species concentration, electrochemical reactions, electric and ionic conduction and heat transfer.

A number of detailed theoretical and numerical models of the coupled electro-chemical, thermal, and fluid processes in SOFCs have been already developed, and published.

Recently, many papers have modelled the SOFC with Subroutines in a commercial computational fluid dynamic software (CFD). Based on 3-D model and time-dependent [1-8], these models are used to foresee the temperature distribution, gas concentration, velocity profile across the cell and current density. The CFD approach demands a great deal of computational power, especially when simulating a long transient process with a large number of parameters to study. Adding to the computational expense is the very fine discretization required for numerical modelling. This is because of the very high scale ratio of components dimensions in the cell (small thickness of component cell).

Another simplifying model based on 2-D [9] calculates the temperature distribution in the fuel and the air streams along the longitudinal direction. This model considers heat and mass transfer characteristics mainly along the longitudinal direction of the system and the electrochemical reaction in its perpendicular direction.

In [10-11], a 1-D model approach is developed only along the flow direction and the radiation heat is taken into account.

[12-14] use the control volume (CV) approach for the tubular geometry. From this modelling technique, the cell is divided in serial segments by planes perpendicular to fuel flow direction. Each segment includes: cell CV, anode CV, cathode CV and insulator CV. The heat transfer, species transportation and electrochemical reaction effects are taken into account.

In this paper, three sub-models have been developed (thermal, fluidic and electrochemical) and coupled. The transient thermal model is used to compute the solid and gas temperatures. The fluidic model calculates the partial pressures of chemical species. The electrochemical model computes the stack voltage and different overvoltages [15].

The figure 1 shows the schematic of stack modelling.

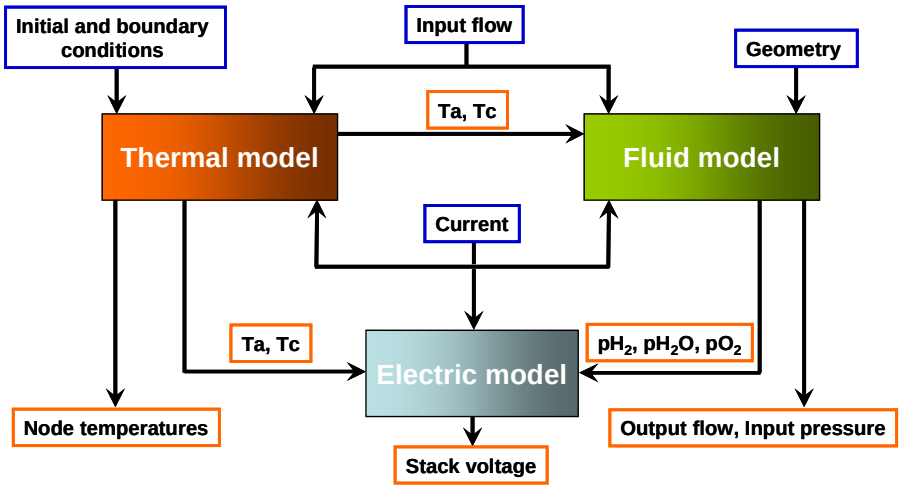

Figure 1 Schematic of stack modelling

2- Thermal modelling

Thermal failure of components in SOFC is a major obstacle on the path to bringing this technology to commercial viability. The probability of material degradation and failure in SOFCs depends strongly on the local temperature gradients at the interfaces of different materials. Therefore, it is important to accurately predict and manage the temperature fields within the stack, especially near the interfaces.

A SOFC involves complicated heat transfer, species transportation, and electrochemical effects which are highly interactive. In order to make the model tractable while capturing the fundamental dynamic behaviour, a model quasi-2D based on the nodal network of one cell has been developed. This method has already been applied to PEMFC [16]. It provides less accurate results than CFD computations [1-8] which are particularly useful to improve the design of the cell. But it require less internal data on the geometry and material and is easier to implement in a global model.

As shown in Figure 2, the cell is divided into several isothermal volumes: anode interconnect, anode channel, electrolyte/anode interface, electrolyte, electrolyte/cathode interface, cathode channel and cathode interconnect [12-13].

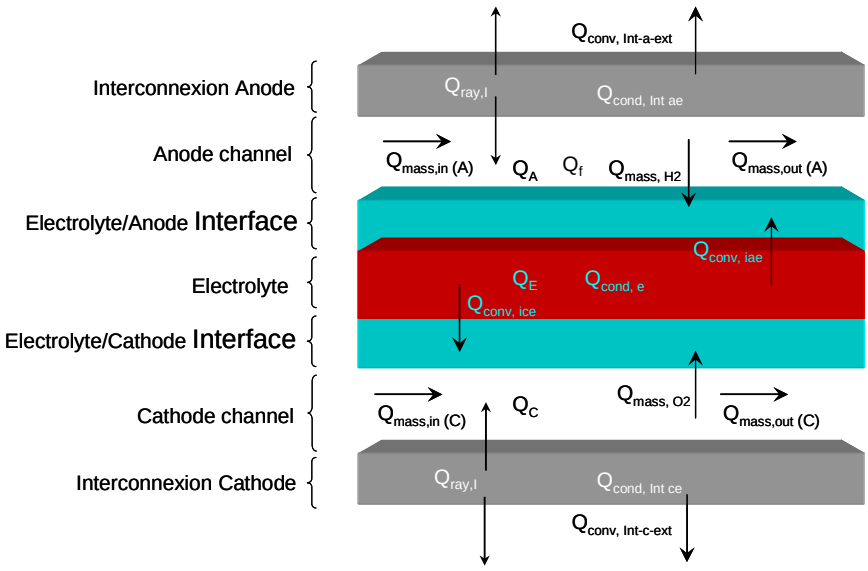

Figure 2 Heat transfer and heat sources on the SOFC cell

The cell is submitted to six fundamental heat transfers:

1- Heat transfer due to mass species transportation: For the anode and cathode channel, the heat generation by gas transportation can be represented as:

$$Q_{mass} = \dot{m} \cdot c_p \cdot \Delta T \quad (1)$$

Where, $\dot{m}$ is the gas mass flow (kg/s), c_p is the heat capacity (J/kg.K) and ΔT is the temperature difference between two nodes [K].

2- Conduction heat transfer: from the solid to solid structures (interconnects and electrolyte), the conduction heat generation is given by:

$$Q_{cond} = \frac{\lambda \cdot S}{e} \Delta T \quad (2)$$

Where, λ is the material thermal conductivity (W/m.K), e is the volume thickness (m) and S is the volume area (m²).

3- Convection heat transfer: from the solid to gas structures, is given by following expression:

$$Q_{conv} = h \cdot S \cdot \Delta T \quad (3)$$

Where, h: is the heat transfer coefficient.

4- Radiation heat transfer: from the solid to solid surface structures, it is calculated by:

$$Q_{conv} = \varepsilon \cdot \sigma \cdot S \cdot \left(T_1^4 - T_2^4\right) \quad (4)$$

Where, ε is the emissivity of the object and σ is the Stefan-Boltzmann coefficient ($5.6703.10^{-8}$ W/m^{2}K^4).

5- The heat generation by chemical reaction: the water formation at anode side is represented as:

$$Q_f = \frac{I}{2F} T \Delta S \quad (5)$$

Where, I is the cell current, T is the cell temperature and ΔS is entropy of the reaction ($\frac{1}{2}O_2 + H_2 \rightarrow H_2O$).

6- Heat generation by ohmic losses: at anode (Q_A), cathode (Q_C) and the electrolyte (Q_E), caused by ohmic resistance:

$$Q_A = R_A \cdot I^2 \quad (6)$$

$$Q_C = R_C \cdot I^2 \quad (7)$$

$$Q_E = R_E \cdot I^2 \quad (8)$$

Where, R_A, R_C and R_E are respectively anode, cathode and electrolyte ohmic resistance.

The ohmic resistance is calculated using the following expression:

$$R = \rho \frac{\delta}{A} \quad (9)$$

Where, δ is the thickness component, A is the area of component and ρ is corresponding to the material resistivity, calculated with temperature-dependent relation [17] (table1).

Table 1 Component resistivity [17]

	Electric or ionic resistivity (Ωcm)
Anode	$0.00298 \exp\left(\frac{-1392}{T}\right)$
Cathode	$0.008114 \exp\left(\frac{500}{T}\right)$
Electrolyte	$10.0 \exp\left(10092\left(\frac{1}{T} - \frac{1}{1273.15}\right)\right)$

The modelling principle by nodal network consists in establishing a co-relation with an electrical network. The considered system is separated into isothermal elements of volume V_i with temperature T_i. Each element "i" has a heat capacity C_i applied to the center i of V_i and possibly a heat power generation. The item "i" is called node of the system (figure 3).

The heat transfers by convection, radiation and conduction and the mass transfers as well are taken into account through the matrix G_{ij}. The heat generation by chemical reaction and ohmic losses are located in the vector Q_i. The heat balance resulting from the first principle of thermodynamics is applied to the node "i":

$$C_i \frac{dT_i}{dt} = \sum_j G_{ij}(T_j - T_i) + Q_i \quad (10)$$

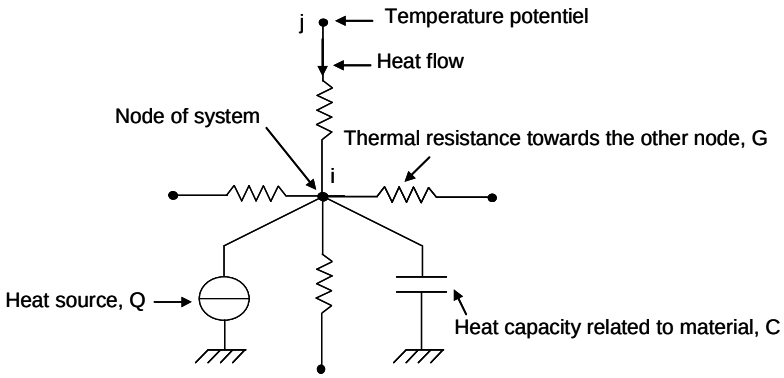

Figure 3 Principal of thermal nodal modelling

The nodal modelling is applied at fifteen nodes on cell. The figure 4 shows a 2D model representation of the studied cell. This last is composed with fifteen isothermal control volumes.

The following heat transfer mechanisms and assumptions have been considered:

1. The heat conduction in solid structures (electrolyte and interconnect), it is represented by green thermal resistance.
2. The heat convection between gases and surfaces of solid structures (ex: hydrogen and interconnect surface), represented by blue thermal resistance.
3. The heat radiation between two solid structures (ex: interconnect and electrolyte), represented by red thermal resistance.
4. The heat generation by mass transfer, represented by black thermal resistance.
5. The heat radiation between gas and solid structure is neglected.

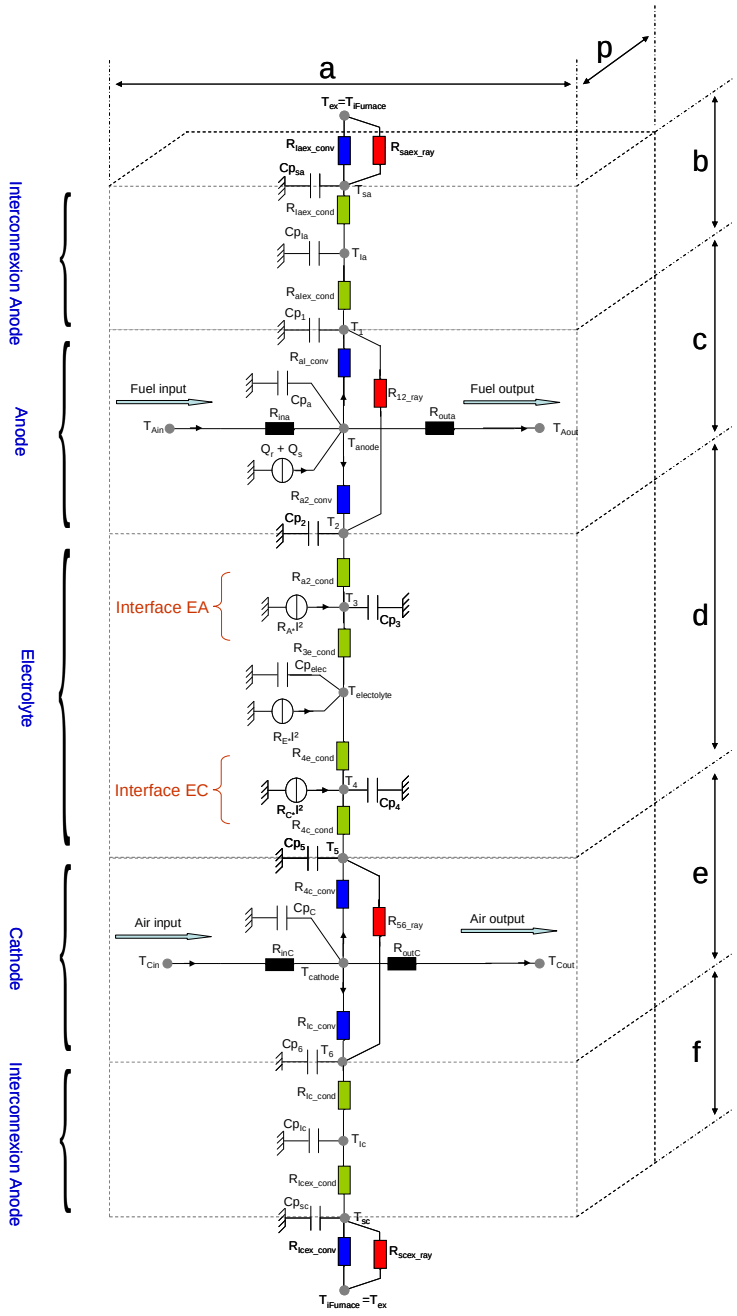

Figure 4 Thermal model of one cell

The energy balance at each node is given (appendix) in order to represent the global energy balance system in the form:

$$C_p \frac{dT}{dt} = A \cdot T + B \qquad (11)$$

Where, T is the temperature vector, C_p is the heat capacity matrix, A is the thermal resistance matrix and B is the heat generation vector.

Figure 5 shows the algorithm of the transient thermal model. At the beginning of the simulation, the cell geometry, physical proprieties (specific heat capacity, thermal conductivity, kinetic viscosity…) and initial temperatures are loaded. In the first step, the Reynolds number is calculated and the Nusselt number is empirically calculated by

correlation equation. The heat transfer coefficient is computed from the Nusselt number for a forced convection between 2 parallel plates by the following expression:

$$h = Nu \cdot \frac{\lambda}{D_h} \qquad (12)$$

Where, Nu is the Nusselt number, λ is the thermal conductivity and D_h is the diameter of channel.

The heat transfer coefficient calculated is high due to the small characteristic length. The values of h, which have been obtained from this forced convection correlation on the air and fuel sides belong to the range 1000-2000 W/m²K for the fuel and 300-1000 W/m²K for the air. These results are consistent with some literature estimation respectively: $h(fuel) = 2987 W/m^2 \cdot K$ and $h(air) = 1322.8 W/m^2 \cdot K$, [12].

For each heat transfer mechanism, the thermal resistances are calculated using the table 2.

Table 2 Thermal resistance calculation

Heat transfer mechanism	Thermal resistance
Heat conduction	$R_{cond} = \frac{e}{\lambda \cdot S}$
Heat convection	$R_{conv} = \frac{1}{h \cdot S}$
Heat radiation	$R_{ray} = \frac{1}{\varepsilon \cdot \sigma \cdot S \cdot \left(T_1^2 + T_2^2\right) \cdot \left(T_1 + T_2\right)}$
Heat mass transfer	$R_{mass} = \frac{1}{m \cdot c_p}$

In the second step, the matrix A, B and C_p are calculated. The Matlab's ODE solver routine is applied and the new temperatures are calculated. The boundary conditions are the inlet temperature of the fluid and the inside temperature of furnace surface. The Runge-Kutta methodology is applied to give the final temperatures vector.

Figure 5 summarizes the algorithm of the transient thermal model.

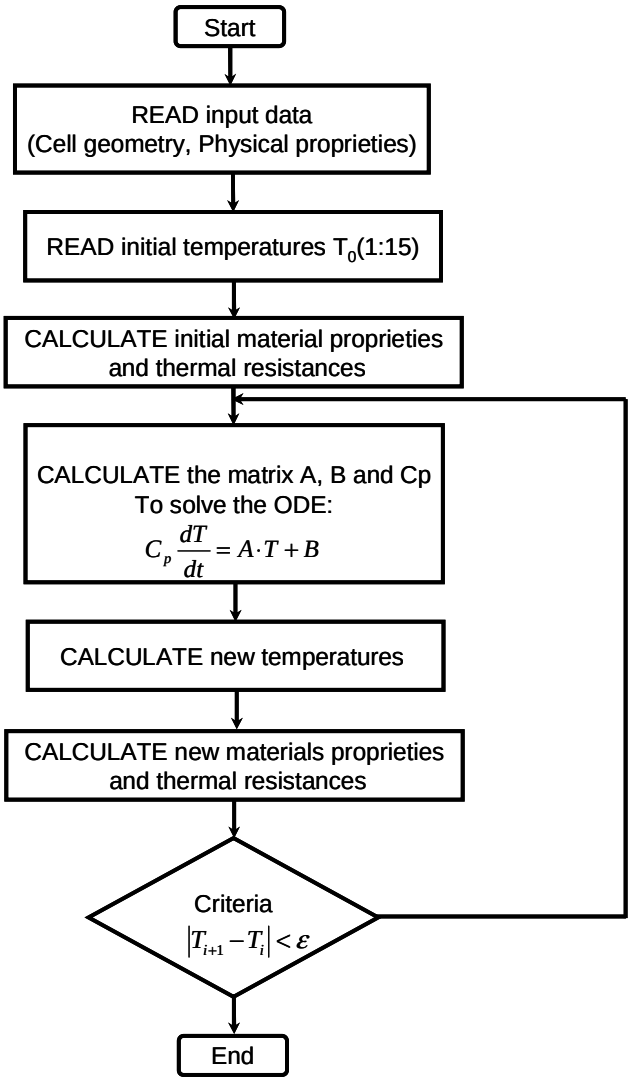

Figure 5 Algorithm of the transient thermal model

3- Fluidic model

The fluidic behaviour in anode and cathode sides has been modelled using an electric fluid analogy [15]. In a formal approach, the flow is related to a current and the pressure is related to a voltage. It is considered that the pressure drop on air side and fuel side is linear with the air flow and fuel flow (table 3) in the considered flow rate range.

Table 3 Electric fluid analogy

Electrical	Fluidic
Voltage (V)	Pressure (mbar)
Current (A)	Volumetric flow rate (Nl/min)
Electrical resistance (Ω)	Fluidic resistance (mbar/Nl.min^{-1})

So, each electrode of volume V is modelled with an electric circuit (figure 6):

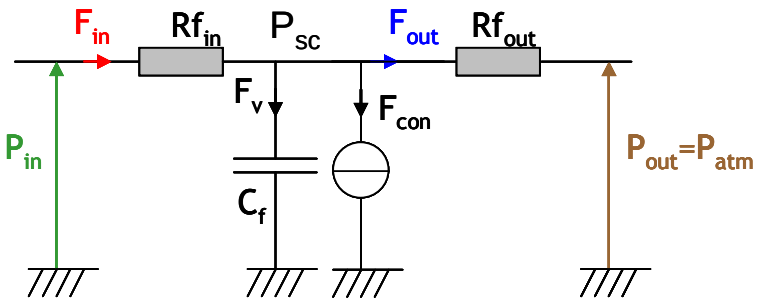

Figure 6 Electrode fluidic model

Where:

F_{in} : input gas flow (Nl/min)

F_{out} : output gas flow (Nl/min)

F_V : buffer gas flow (Nl/min)

F_{con} : consumed gas flow (Nl/min)

P_{in} : inlet gas pressure (mbar)

P_{out} : outlet gas pressure (mbar)

P_{sc} : pressure (catalytic site sc) (mbar)

R_{fin} : fluidic resistance (mbar/Nl.min^{-1})

R_{fout} : electrode/electrolyte interface downstream fluidic resistance (mbar/Nl.min^{-1})

C_f : fluidic capacity (C_f=V/RT) (mbar^{-1})

The fluidic model will be based on the following assumptions:

- The gases are ideal.
- The gas flowing in anode side and cathode side have the same direction (co-flow).
- The channels (anode and cathode) have a fixed volume.
- Consumption and accumulation of fluids are modelled in one point.

4- Measurements and identification

4-1 Characteristic of the tested stack

Tests have been performed on a SOFC stack in order to identify parameters of the model which has been developed. A test bench has been realized with a 3 cell stack provided by HTceramix company. The stack is fed by hydrogen and air and the gas flow rates are kept constant.

The table 4, shows the characteristics of the HTceramix stack [18].

Table 4 HTceramix stack specifications and operating conditions

Number of cells in stack	3
Active area per cell	50 cm²
Ideal operating temperature	750°C

Max operating temperature	800°C
Air flow rate	4.3 l/min
Hydrogen flow rate	0.9 l/min
Nominal power density	> 0.4W/cm²
Max pressure drop on air side	20 mbar
Max pressure drop on fuel side	10 mbar

4-2 Fluidic resistance identification

When the stack is operated at open circuit voltage (OCV) and fed with constant gas flow rate, the consumed gas flow and the flow variation in the electrode volume are negligible. So, the inlet gas flow and outlet gas flow are equal. The input and output resistances are also calculated by following expression:

$$Rf_{in}(I = 0A) = Rf_{out}(I = 0A) = \frac{\Delta P}{2 \cdot F} \qquad (13)$$

ΔP : the pressure drop in flow channels (mbar)

F : the gas flow (Nl/min)

The stack is fed with constant gas flow given in table 4, figures 7-8 show the experimental data: the stack voltage, the gas temperatures and the fluidic resistance variation with temperature.

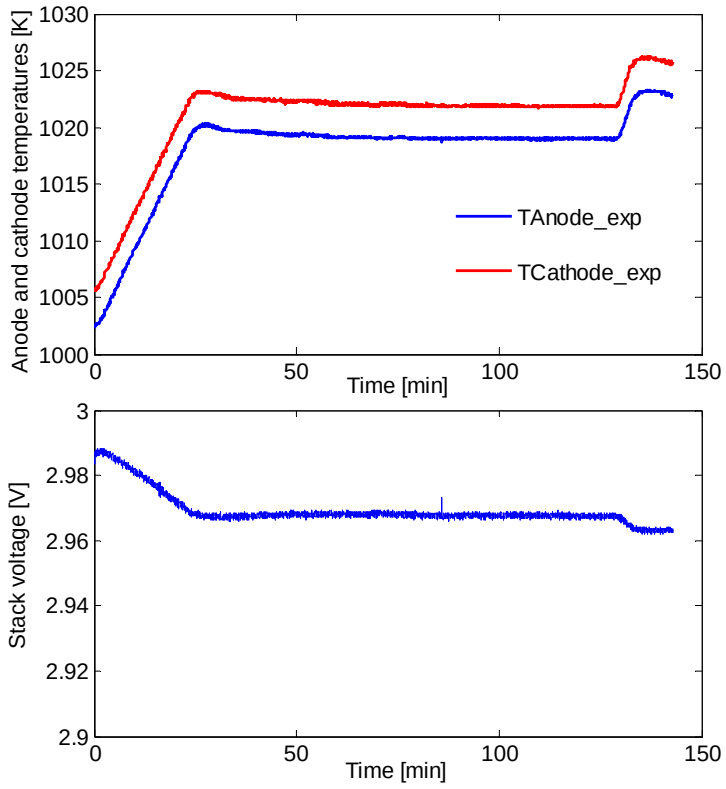

Figure 7 Experimental data at OCV

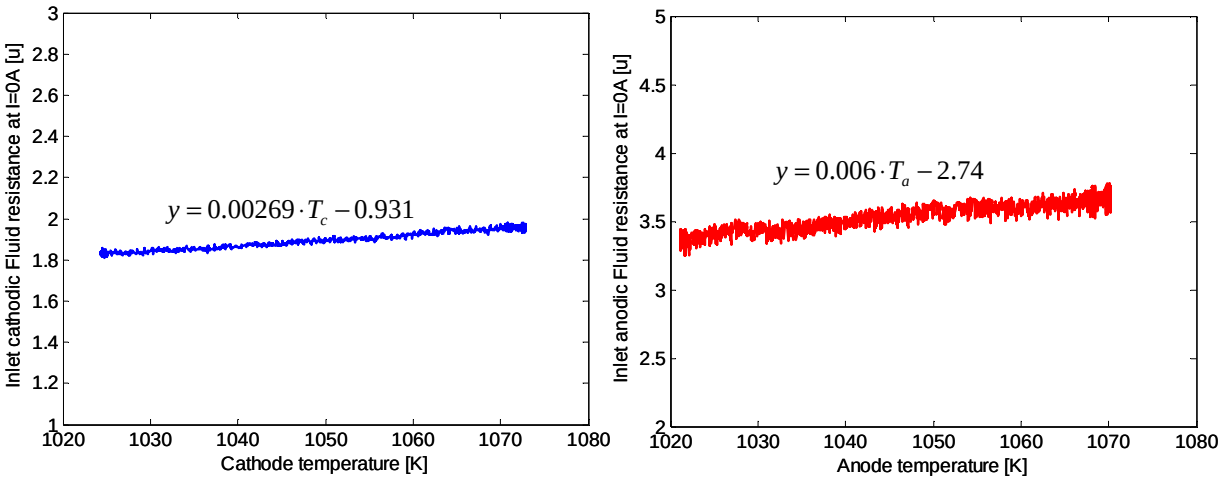

Figure 8 Inlet cathodic and anodic fluid resistance at OCV calculated from experimental data and its fitting

In order to calculate the fluid resistances at different current loads, polarization curves are realised with increasing and decreasing currents, at constant temperature and constant inlet gas flows. The figures 9-11 show the polarization curve, the inlet gas temperature taken as electrode temperature and the gas pressures.

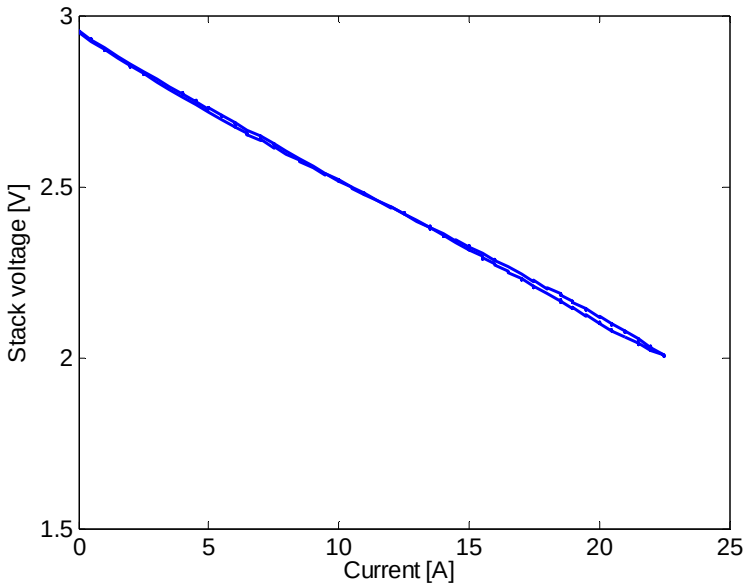

Figure 9 Polarization curve with increasing and decreasing current at (T_a=750°C)

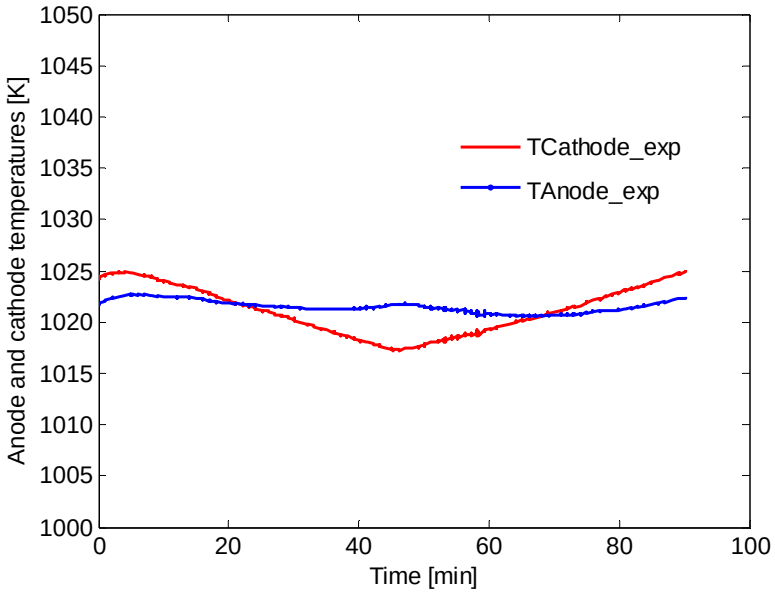

Figure 10 Anode and cathode temperatures (inlet gas temperatures)

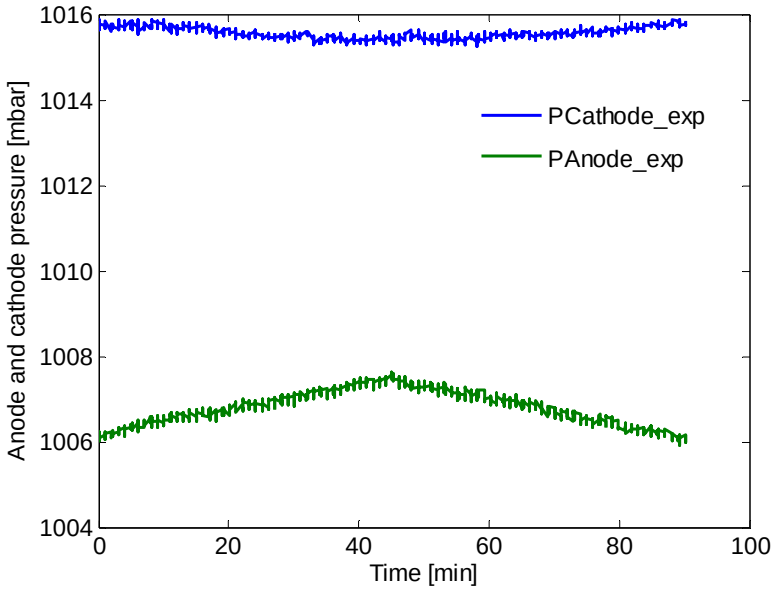

Figure 11 Anode and cathode pressures

The anodic and cathodic fluidic resistances are function of the temperature and current load (14-17).

$$Rf_{a,in} = 0.006 \cdot \mathrm{T_a} - 2.74 \quad (14)$$

$$Rf_{a,out} = 0.006 \cdot \mathrm{T_a} - 2.74 + 0.5 \cdot I \quad (15)$$

$$Rf_{c,in} = 0.00269 \cdot \mathrm{T_c} - 0.931 \quad (16)$$

$$Rf_{c,out} = 0.00269 \cdot \mathrm{T_c} - 0.931 + 3.5 \cdot I \quad (17)$$

4-3 Fluidic capacity identification

The gases which circulate in the anode and cathode channels are considered ideal and the channel volumes are taken constant. The identification method is presented at the anode. The gas partial pressure at the anode and electrolyte interface (noted catalytic site) can be calculated from the following relationships [15,19,20]:

$$p_{sc,H2} \cdot V_a = n_{v,H2} \cdot R \cdot T_a \tag{18}$$

$$n_{v,H2} = \int D_{v,H2} \cdot dt = \int \left(D_{in,H2} - D_{out,H2} - D_{con,H2} \right) \cdot dt = \frac{V_a}{R \cdot T_a} \cdot p_{sc,H2} \tag{19}$$

$$p_{sc,H2} = \frac{1}{\frac{V_a}{R \cdot T_a}} \int D_{v,H2} \cdot dt \tag{20}$$

Where, $D_{v,H2}$ is the hydrogen molar flow in the anodic volume.

Using the fluidic electric analogy (table 3), the fluidic capacity is calculated using the following expression:

$$C_{f,a} = \frac{V_a}{R \cdot T_a} \tag{21}$$

$$C_{f,c} = \frac{V_c}{R \cdot T_c} \tag{22}$$

Figures 12-13 show the block diagram of the anode fluidic model developed in Matlab Simulink. The hydrogen consumption and the water production flows are computed from the stack current according to the Faraday law.

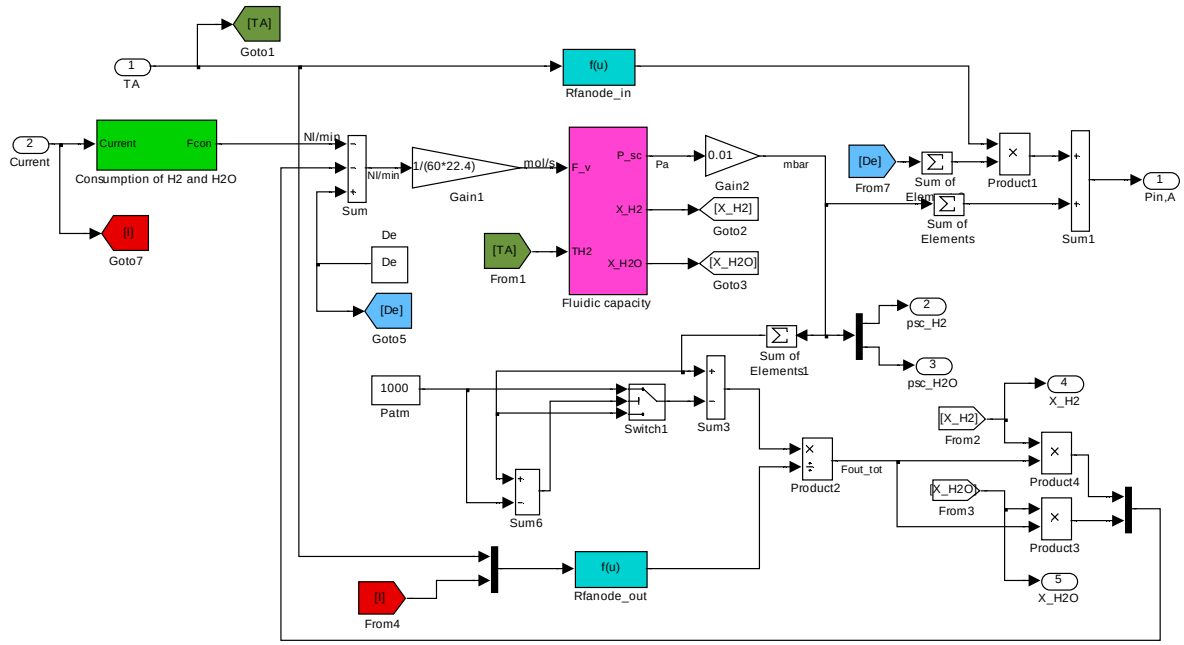

Figure 12 Block diagram of the anode

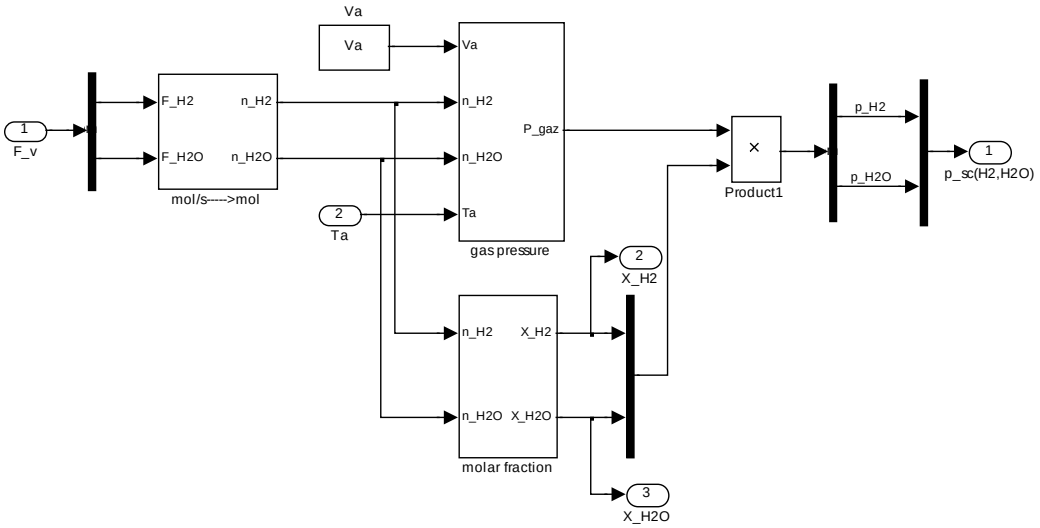

Figure 13 Fluidic capacity of the anode

5- Electrochemical model

The SOFC is operated with pure hydrogen and air. So, the electrochemical reactions to be considered are (23-25):

$$O_2 + 4e^- \rightarrow 2O^{2-} \quad (23)$$

$$H_2 + O^{2-} \rightarrow H_2O + 2e^- \quad (24)$$

$$H_2 + \frac{1}{2}O_2 \rightarrow H_2O \quad (25)$$

The stack voltage is computed using the following equation [21-26]:

$$U_{stack} = N_{cell} \cdot (OCV - \eta_{ohm} - \eta_{con} - \eta_{act}) \quad (26)$$

Where N_{cell} is the number of cells in the stack and the other four terms represent respectively, the open circuit voltage, the ohmic, concentration and activation overvoltages.

5-1 Open circuit voltage

The OCV is calculated using Nernst equation:

$$OCV = E^0 + \frac{RT}{2F}\ln\left(\frac{p_{H2}p_{O2}^{0.5}}{p_{H2O}}\right) \quad (27)$$

$$E^0 = \frac{-\Delta G^0}{2F} \quad (28)$$

Where E^0, the reversible voltage for hydrogen oxidization at ambient pressure, ΔG^0 represents the standard Gibbs free energy change in the overall cell reaction under standard condition (T=25°C and P=1atm), R is ideal gas constant, p is the partial pressure of the reactants and products and F is the Faraday constant.

The Gibbs free energy at standard conditions may be calculated from the Gibbs free energies of formation of the products and reactants from equation (25).

The reversible voltage as a function of temperature at cell reaction sites limited to the first order ([4,27,28]):

$$E^0 = 1.273 - 2.7645 \cdot 10^{-4} \cdot T \quad (29)$$

The temperature (T) and partial pressures (p_i) are respectively calculated by thermal model and fluidic model.

5-2 Activation overvoltage

The activation overvoltage describes the resistance to charge transfer at each of the half cells. It is the principal source of losses at low current densities. The expression of the activation overvoltage ([11,15,20]) is calculated by:

$$\eta_{act} = \frac{RT}{\alpha nF} Ln\left(\frac{i}{i_0}\right) \quad (30)$$

Where:

α : Electron transfer coefficient

n : Number of electron

i : Current density [A/cm²]

i_0 : Exchange current density [A/cm²]

We can write over an empirical equation:

$$\eta_{act} = aLn(i) + b \quad (31)$$

With:

$$a = \frac{RT}{\alpha nF}$$

$$b = -\frac{RT}{\alpha nF} Ln(i_0)$$

The coefficients a and b are functions of temperature and are calculated empirically.

5-3 Ohmic overvoltage

The ohmic overvoltage is caused by the resistance to the conduction of ions O^{2-} (through the electrolyte) and electrons (through the electrodes and the current collector) and by the contact between the cell components.

The ohmic overvoltage is calculated used the following expression:

$$\eta_{ohm} = R_{ohm} \cdot I \quad (32)$$

Where, R_{ohm} is the ohmic resistance and I is the stack current.

The ohmic resistance is only function of stack temperature:

$$R_{ohm} = A \cdot \exp\left(B \cdot T^{-1}\right) \quad (33)$$

Where, T is the stack temperature, A and B are calculated in the linear part of the polarization curves.

5-4 Concentration overvoltage

The concentration overvoltage describes the losses due to gas transport losses in the cell. They are the principal source of losses at high current densities, it is calculated by the following expression:

$$\eta_{con} = \frac{RT}{nF} Ln\left(1 - \frac{i}{i_L}\right) \quad (34)$$

Where:

i_L : limiting current [A]

6- Results

In all the tests, the anode side is fed with pure hydrogen and the cathode is fed with air. The gas flows are taken constant at the following values: the hydrogen flow (F_{inH2}) is 0.9 Nl/min, and the air flow (F_{inAir}) is 4.3 Nl/min.

The figure 14 shows the simulation result of the thermal model at very low current (about 1A) : fifteen node temperatures are given, the name of the nodes are related to the figure 4. The model inputs are: the inlet hydrogen temperature, the inlet air temperature and the furnace temperature, they are respectively 1010K, 974K and 1037K.

The convection heat transfer coefficient of hydrogen is high and the radiation effect between the electrolyte and the interconnect occurs. Hence, in the simulation results, the temperature of the node (T_{anode}) in the middle of the anode channel (figure 14) is the highest one.

The simulation results show two thermal responses: the zone 1 which consists in the material interconnect (T_{sa}, T_{Ia}, T_1 nodes of the anode interconnect and T_{sc}, T_{Ic}, T_6 nodes of the cathode interconnect) with high thermal conductivity and the zone 2 which consists in the electrolyte and the gas in the channels with low thermal conductivity.

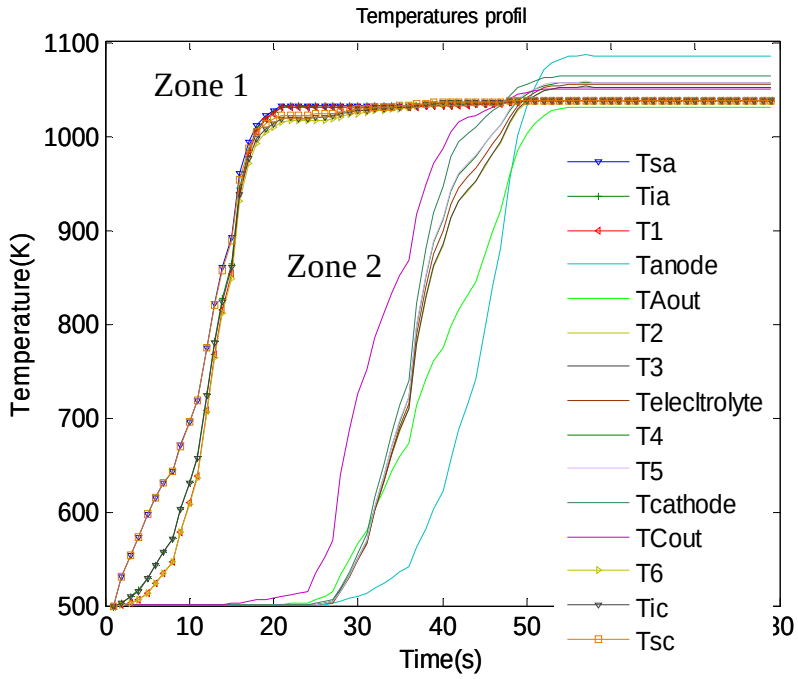

Figure 14 Simulation result of thermal model

As temperature measurements inside the stack are not available, the validation of the thermal model is made on the output gas temperature. The figures 15 and 16 show the comparison of the simulation results with experimental data in the same operating conditions than in fig. 14.

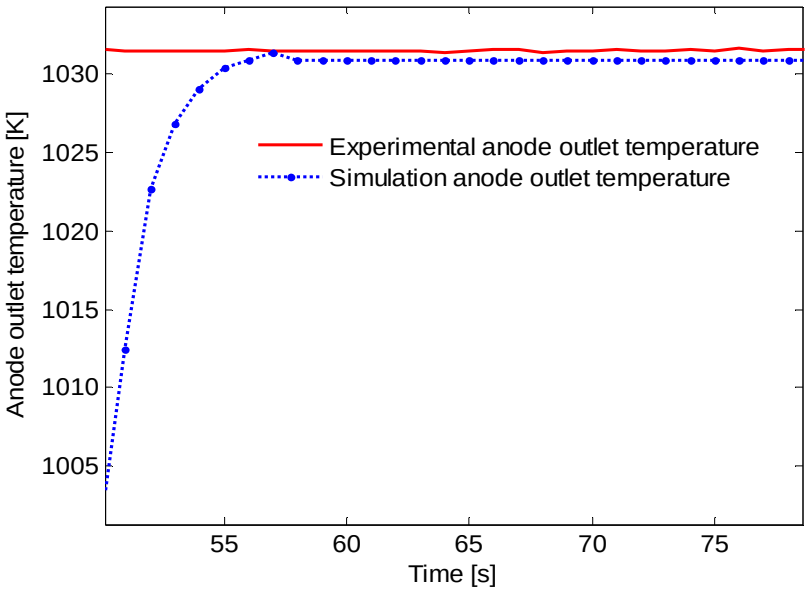

Figure 15 Hydrogen outlet temperature validation

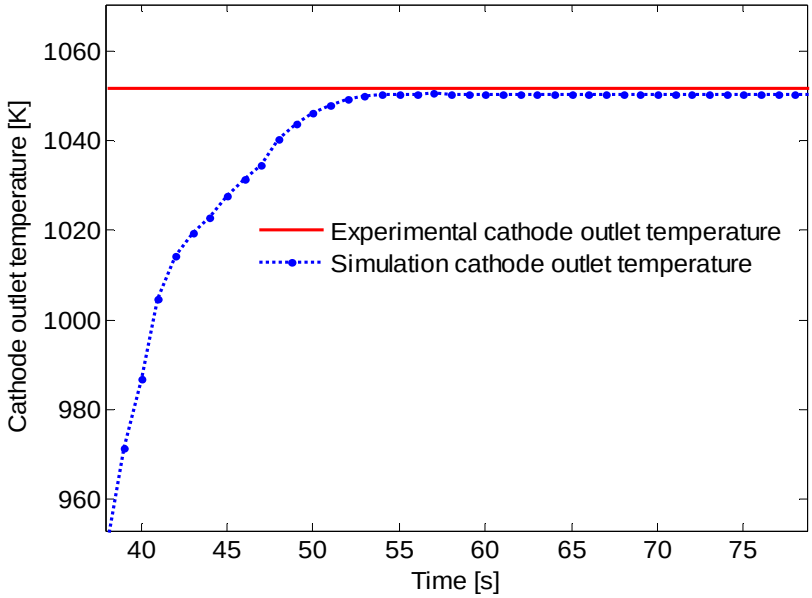

Figure 16 Air outlet temperature validation

The figure 17 shows the validation of the polarization curves. At average current range where the ohmic drop is dominating, the model follows exactly the experimental results. At low current, where activation overvoltages are dominating, a light difference can be noticed between the model and the experimental because of the low acquisition frequency of the test bench which does not give enough points at low current.

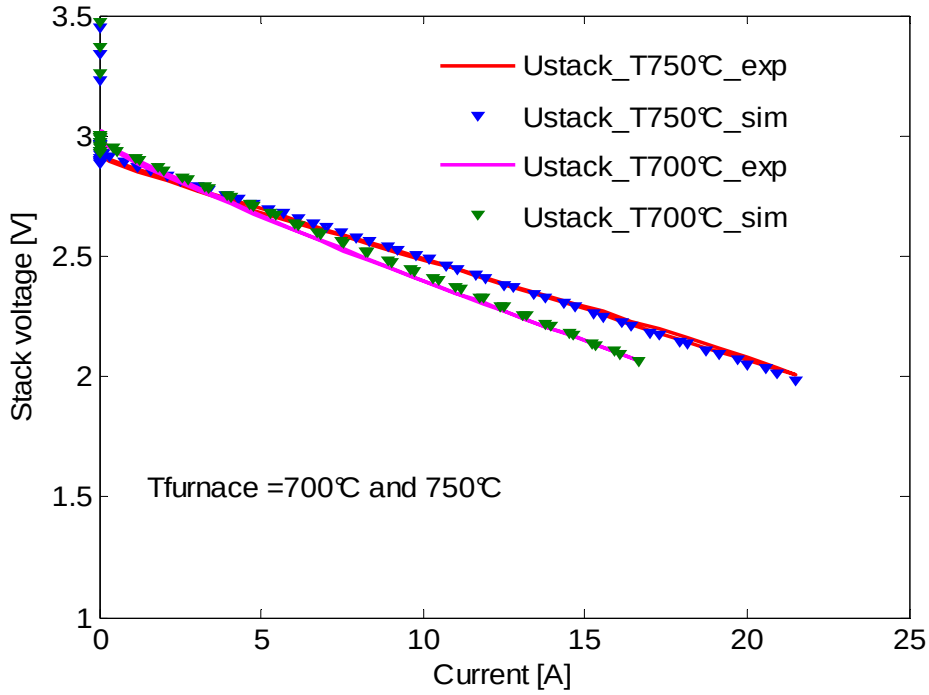

Figure 17 Polarization curves validated

In order to validate the fluidic model, figures 19-22 show the simulation and experimental

comparison. The load current profile of figure 18 is applied. Increasing and decreasing step currents are used: 0.5 A step then a 1min stabilisation.

The experimental anode and cathode inlet pressures are similar to the simulation (figures 19-20), and the variation law of fluidic resistances is confirmed.

On the anode side, the water formation reaction increases the partial pressure of water and the reduction of the hydrogen mole number due to the reaction taking place in the anode/electrolyte interface causes a reduction of the hydrogen partial pressure.

In the cathode side, the oxygen is consumed in the chemical reaction which justifies the diminution of the oxygen partial pressure in the cathodic compartment and the nitrogen is not consumed in cathode side, so its partial pressure increases.

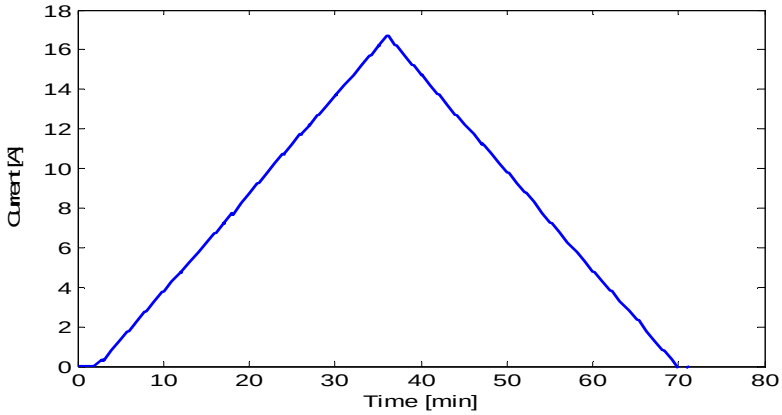

Figure 18 Current profil

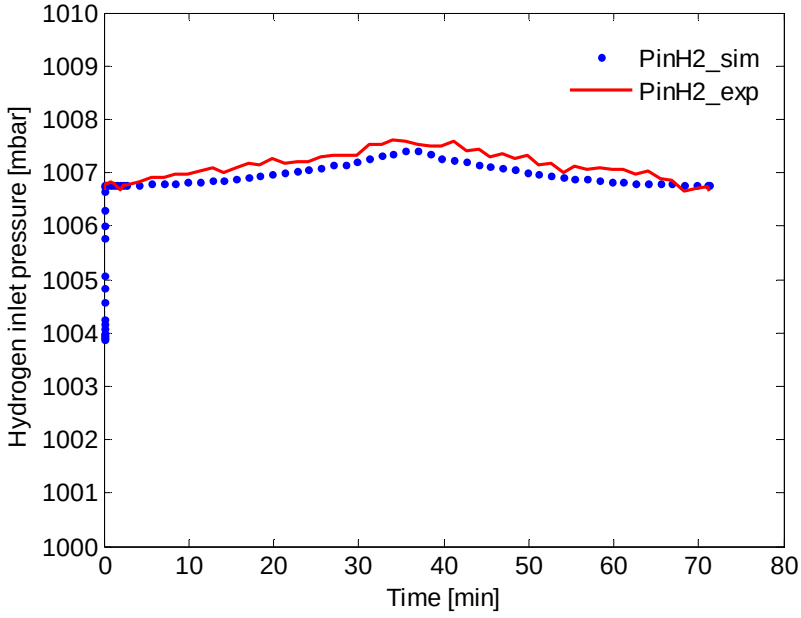

Figure 19 Anode inlet pressure validation

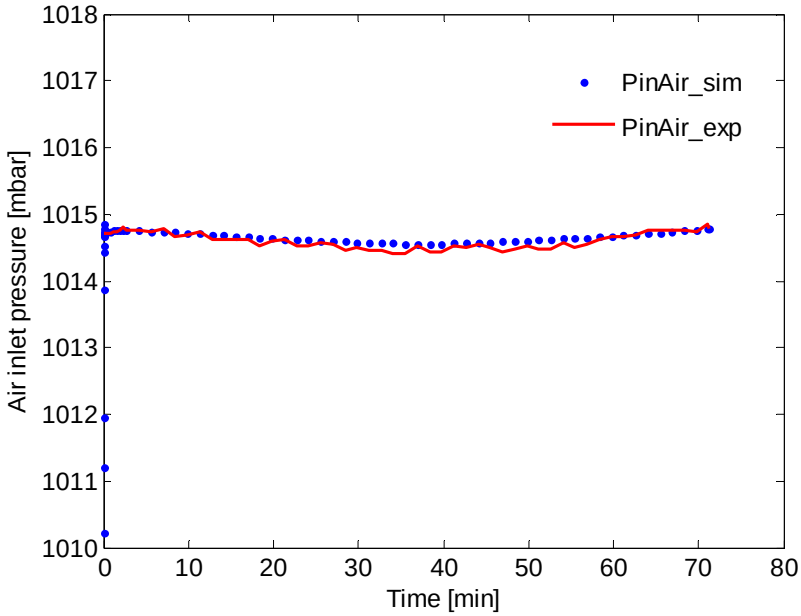

Figure 20 Cathode inlet pressure validation

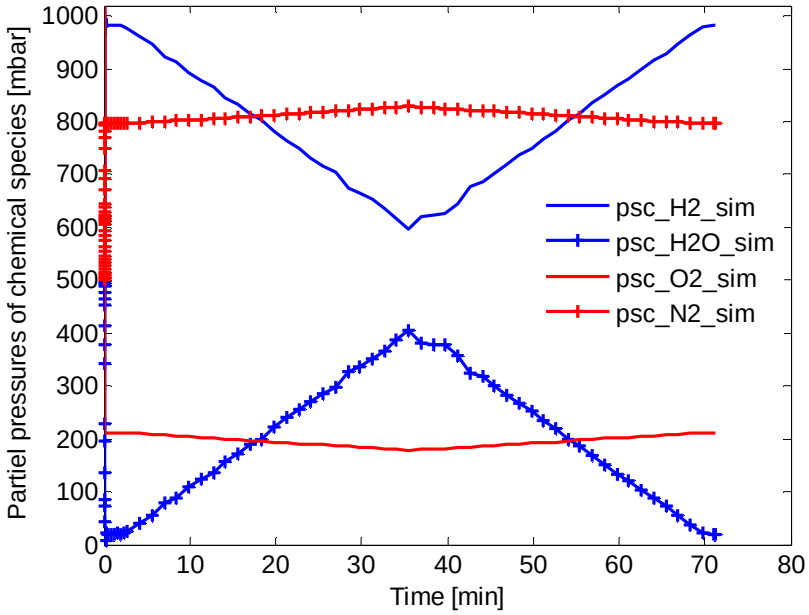

Figure 21 Partial pressure of chemical species

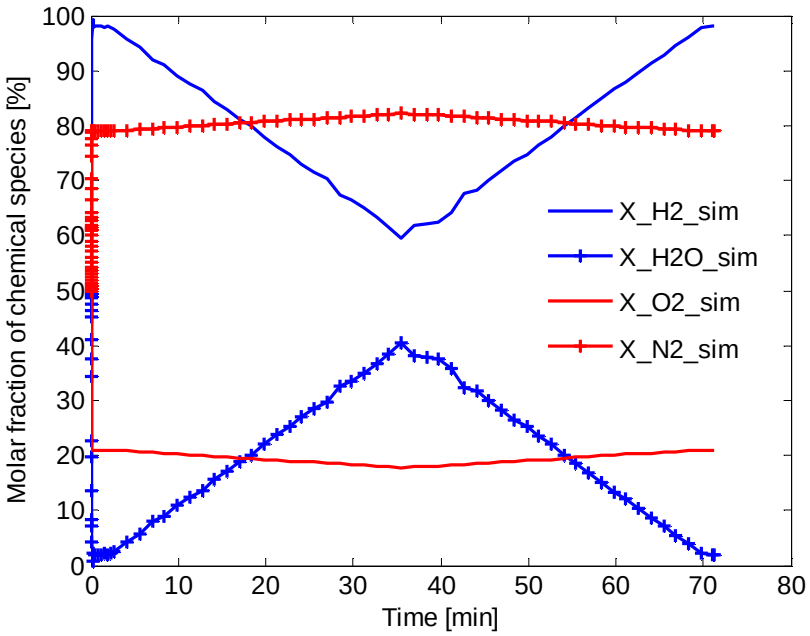

Figure 22 Molar fraction of chemical species

7- Conclusion

In this paper, a simulation of a SOFC combining thermal, fluidic and electrochemical models is developed.

The potential and reliability of the model developed has been shown. The inside temperatures of the gases and different control volumes are computed by the thermal model. Partial pressure calculation is given by the fluidic model and the stack voltage is provided by the electrochemical model.

It can be concluded that the developed model is an interesting tool for the simulation of fuel cell power supply. Due to the compromise which has been chosen between accuracy, fuel cell manufacturer know-how data and computation time, it can be easily implemented in a global modelling with additional components (fuel cell auxiliaries, energy buffers, etc). The first application will be the simulation of the coupling of an SOFC and a PEFC.

References

[1] E. Achenbach, Three-dimensional and time-dependent simulation of a planar solid oxide fuel cell stack, Journal of Power Sources, 49 (1994) 333–348

[2] H. Yakabe, T. Ogiwara, M. Hishinuma and I. Yasuda, 3-D model calculation for planar SOFC, Journal of Power Sources, 102 (2001) 144–154.

[3] N. Autissier, D. Larrain, J. Van herle and D. Favrat, CFD simulation tool for solid oxide fuel cells, Journal of Power Sources, 131 (2004) 313-319

[4] K. Sudaprasert, R.P Travis and R.F Martinez-Bots, A computational fluid dynamic model of a solid oxide fuel cell, Imperial college of London, Department of Mechanical Engineering, London UK, Proc. IMechE Vol. 219 Part A: J. Power and Energy, IMechE 2005

[5] J.R. Ferguson, J. M Fiard and R. Herbin, Threedimensional numerical simulation for various geometries of solid oxide fuel cells, Journal of Power Sources, 58 (1996) 109–122

[6] L. Petruzzi, S. Cocchi, F. Fineschi, A global thermo-electrochemical model for SOFC systems design and engineering, Journal of Power Sources, 118 (2003) 96–107

[7] K. P. Recknagle, R.E. Williford, L.A. Chick, D.R. Rector, and M. A. Khaleel, Three-dimensional thermofluid electrochemical modelling of planar SOFC stacks, Journal of Power Sources, 113 (2003) 109–114

[8] M.A. Khaleel, Z. Lin, P. Singh, W. Surdoval, D. Collin, A finite element analysis modeling tool for solid oxide fuel cell development: coupled electrochemistry, thermal and flow analysis in MARC, Journal of Power Sources, 130 (2004) 136–148

[9] Tae Won Song, Jeong Lak Sohn, Jae Hwan Kim, Tong Seop Kim, Sung Tack Ro, Kenjiro Suzuki, Performance analysis of a tubular solid oxide fuel cell/micro gas turbine hybrid power system based on a quasi-two dimensional model, Journal of Power Sources, 142 (2005) 30–42

[10] L. Damm David, G. Fedorov Andrei, Reduced-order transient thermal modeling for SOFC heating and cooling, Journal of Power Sources, 159 (2006) 956–967

[11] H. Chan, K. Khor and Z. Xia, A complete polarization model of a solid oxide fuel cell and its sensitivity to the change of cell component thickness. Journal of Power Sources, 93 (2001) 130–140

[12] X. Xue, J. Tang, N. Sammes, Y, Du, Dynamic modeling of single tubular SOFC comining heat/mass transfer and electrochemical reaction effects, Journal of Power Sources, 142 (2005) 211-222

[13] Susumu Nagata, Akihiko Momma, Tohru Kato, Yasuhiro Kasuga, Numerical analysis of output charateristics of tubular SOFC with internal reformer, Journal of Power Sources, 101 (2001) 60-71

[14] C. Haynes, Simulating process settings for unslaved SOFC response to increases in load demand, Journal of Power Sources, 109 (2002) 365–376

[15] Moussa Chnani, Marie-Cécile Péra, Raynal Glises and Jean-Marie Kauffmann, Macroscopic Model of Solid Oxide Fuel Cell Stack for Integrating in a Generator Simulation, 7th European SOFC Forum, Lucerne, Switzerland, July 2006

[16] L.Dumercy, R.Glises, H.Louahlia-Gualous, J.M.Kauffmann, Transient thermal computation of a PEM fuel cell by a nodal modelling, *VTC'03 Fall*, nov 2003, Orlando (USA)

[17] Pei-Wen Li, Minking K. Chyu, Simulation of the chemical/electrochemical reactions and heat/mass transfer for a tubular SOFC in a stack, Journal of Power Sources, 124 (2003) 487–498

[18] http://www.htceramix.ch/

[19] J. Padullés, G.W. Ault, J.R. McDonald, An integrated SOFC plant dynamic model for power systems simulation, Journal of Power Sources, 86 (2000) 495-500

[20] Kourosh Sedghisigarchi, Ali Feliachi, Dynamic and Transient Analysis of Power Distribution Systems With Fuel Cells-Part I: Fuel- Cell Dynamic Model, IEEE Transactions on Energy Conversion, vol. 19, No. 2, June 2004

[21] David J. Hall, R. Gerald Colclaser, Transient modelling and simulation of tubular solid oxide fuel cell, IEEE Transactions on Energy Conversion, vol. 14, No. 3, September 1999

[22] S. Campanari, P. Iora, Definition and sensitivity analysis of a finite volume SOFC model for a tubular cell geometry, Journal of Power Sources, 132 (2004) 113–126

[23] Yutong Qi, Biao Huang, Karl T. Chuang, Dynamic modeling of solid oxide fuel cell: The effect of diffusion and inherent impedance, Journal of Power Sources, 150 (2005) 32-47

[24] Larminie, J. and Dicks, A. Fuel Cell Systems Explained, 2001 (John Wiley & Sons, Chichester)

[25] S. H. Chan, H. K. Ho, and Y. Tian, Modelling of simple hybrid solid oxide fuel cell and gas turbine power plant, Journal of Power Sources, 109 (2002) 111–120

[26] Paola Castamagna, Azra Selimovic, Marc Del Borghi, Gerry Agnew, Electrochemical model of integrated planar solid oxide fuel cell (IP-SOFC), Journal of Power Sources, 102 (2004) 61-69

[27] Anon., Fuel Cell Handbook, 5th ed., US Department of Energy, October 2000

[28] Subhash C Singhal and Kevin Kendall, High Temperature Solid Oxide Fuel Cells Fundamentals, Design and Applications, Elsevier Advanced Technolgy, 2003

Appendix

Nomenclature

Variable name	Description	Units
$h_{I,amb}$	Convection heat-transfer coefficient (between interconnect and ambient air)	W/m².K
$h_{A,I}$	Convection heat-transfer coefficient (between anode and interconnect)	W/m².K
$h_{A,elec}$	Convection heat-transfer coefficient (between anode and electrolyte)	W/m².K

$h_{C,elec}$	Convection heat-transfer coefficient (between cathode and electrolyte)	W/m².K
$h_{C,I}$	Convection heat-transfer coefficient (between cathode and interconnect)	W/m².K
λ_1	Interconnect thermal conductivity	W/m.K
λ_2	Electrolyte thermal conductivity	W/m.K
$\dot{m}_a$	The hydrogen mass flow	Kg/s
$\dot{m}_c$	The air mass flow	Kg/s
$R_{ij,cond}$	Thermal resistance by conduction between i and j node	K/W
$R_{ij,conv}$	Thermal resistance by convection between i and j node	K/W
$R_{ij,ray}$	Thermal resistance by radiation between i and j node	K/W
R_{ina}	Thermal resistance by hydrogen mass transfer between the inlet and the middle of the anode	K/W
R_{outa}	Thermal resistance by hydrogen mass transfer between the middle and the output of the anode	K/W
R_{inc}	Thermal resistance by hydrogen mass transfer between the inlet and the middle of the cathode	K/W
R_{outc}	Thermal resistance by hydrogen mass transfer between the middle and the output of the cathode	K/W
R_A, R_C, R_E	Ohmic resistance of anode, cathode and electrolyte	Ω
Q_s	Heat generation by shifting reaction	W
Q_r	Heat generation by reformer reaction	W
Q_f	Heat generation by water formation reaction	W
$C_{p,A}$	Heat capacity of the anode	J/kg.K
$C_{p,C}$	Heat capacity of the cathode	J/kg.K
$C_{p,elec}$	Heat capacity of the electrolyte	J/kg.K
$C_{p,I}$	Heat capacity of the interconnect	J/kg.K
$c_{p,H2}$	Specific heat capacity of the hydrogen	W/kg.K

$c_{p,Air}$	Specific heat capacity of the air	W/kg.K
T_a	Anode temperature	K
T_c	Cathode temperature	K
T_{ex}	Temperature of furnace surface (boundary condition)	K
T_j	Temperature at node j	K
$Rf_{a,in}$	Input anodic fluid resistance	mbar/Nl.min^{-1}
$Rf_{a,out}$	Output anodic fluid resistance	mbar/Nl.min^{-1}
$Rf_{c,in}$	Input cathodic fluid resistance	mbar/Nl.min^{-1}
$Rf_{c,out}$	Output cathodic fluid resistance	mbar/Nl.min^{-1}
V_a	Anode volume	m^3
V_c	Cathode volume	m^3
$p_{in,i}$	Input partial pressure of the i chemical specie	mbar
$p_{out,i}$	Output partial pressure of the i chemical specie	mbar
$p_{sc,i}$	Partial pressure in catalytic site of the i chemical specie	mbar
$F_{in,i}$	Input flow rate of the i specie	Nl/min
$F_{out,i}$	Output flow rate of the i specie	Nl/min
$F_{v,i}$	Flow rate in channel volume v of the i specie	Nl/min
$F_{con,i}$	Reaction flow rate of the i reactant	Nl/min
$C_{f,a}$	Fluidic capacity of the anode	mbar^{-1}
$C_{f,c}$	Fluidic capacity of the cathode	mbar^{-1}
R	Gas constant (8.31)	J/mol.K
$n_{in,i}$	Input molar of the i specie	mol
$D_{in,i}$	Input molar flow rate of the i specie	mol/s
$D_{out,i}$	Output molar flow rate of the i specie	mol/s
$D_{v,i}$	Molar flow rate in the channel volume of the i specie	mol/s
$D_{con,i}$	Reaction molar flow rate of the i reactant	mol/s

The energy balances of thermal model

- Temperature between anode interconnect and furnace (T_{sa}):

$$h_{I,amb}\cdot a\cdot p(T_{ext}-T_{sa})+\varepsilon\cdot\sigma\cdot a\cdot p(T_{ext}^2+T_{sa}^2)(T_{ext}+T_{sa})(T_{ext}-T_{sa})+\frac{\lambda_1\cdot a\cdot p}{b/2}(T_{Ia}-T_{sa})=$$

$$\rho\cdot a\cdot b/4\cdot p\cdot C_{p,I}\frac{\partial T_{sa}}{\partial t}$$

- Middle anode interconnect temperature (T_{Ia}):

$$\frac{\lambda_1\cdot a\cdot p}{b/2}(T_{sa}-T_{Ia})+\frac{\lambda_1\cdot a\cdot p}{b/2}(T_1-T_{Ia})=\rho\cdot a\cdot b/2\cdot p\cdot C_{p,I}\frac{\partial T_{Ia}}{\partial t}$$

- Temperature between anode interconnect and anode (T_1):

$$\frac{\lambda_1\cdot a\cdot p}{b/2}(T_{Ia}-T_1)+h_{A,I}\cdot a\cdot p(T_a-T_1)+\varepsilon\cdot\sigma\cdot a\cdot p(T_2^2+T_1^2)(T_2+T_1)(T_2-T_1)=\rho\cdot a\cdot b/4\cdot p\cdot C_{p,I}\frac{\partial T_1}{\partial t}$$

- Middle anode temperature (T_a):

$$h_{A,I}\cdot a\cdot p(T_1-T_a)+h_{A,elec}\cdot a\cdot p(T_2-T_a)+\dot{m}_A\,c_{p,H2}(T_{Ain}-T_a)+\dot{m}_a\,c_{p,H2}(T_{Aout}-T_a)+Q_r+Q_s+Q_f=$$

$$\rho\cdot a\cdot c\cdot p\cdot C_{p,A}\frac{\partial T_a}{\partial t}$$

- Temperature between anode and anode/electrolyte interface (T_2):

$$h_{A,elec}\cdot a\cdot p(T_a-T_2)+\frac{\lambda_2\cdot a\cdot p}{d/20}(T_3-T_2)+\varepsilon\cdot\sigma\cdot a\cdot p(T_1^2+T_2^2)(T_1+T_2)(T_1-T_2)=$$

$$\rho\cdot a\cdot(d/20)\cdot p\cdot C_{p,elec}\frac{\partial T_2}{\partial t}$$

- Anode/electrolyte interface temperature (T_3):

$$\frac{\lambda_2\cdot a\cdot p}{d/20}(T_2-T_3)+\frac{\lambda_2\cdot a\cdot p}{9d/20}(T_{elec}-T_3)+R_A\cdot I^2=\rho\cdot a\cdot(d/20)\cdot p\cdot C_{p,elec}\frac{\partial T_3}{\partial t}$$

- Electrolyte temperature (T_{elec}):

$$\frac{\lambda_2\cdot a\cdot p}{9d/20}(T_3-T_{elec})+\frac{\lambda_2\cdot a\cdot p}{9d/20}(T_4-T_{elec})+R_E\cdot I^2=\rho\cdot a\cdot(4d/5)\cdot p\cdot C_{p,elec}\frac{\partial T_{elec}}{\partial t}$$

- Cathode/electrolyte interface temperature (T_4):

$$\frac{\lambda_2\cdot a\cdot p}{d/20}(T_5-T_4)+\frac{\lambda_2\cdot a\cdot p}{9d/20}(T_{elec}-T_4)+R_C\cdot I^2=\rho\cdot a\cdot(d/20)\cdot p\cdot C_{p,elec}\frac{\partial T_4}{\partial t}$$

- Temperature between cathode/electrolyte interface (T_5):

$$h_{C,elec}\cdot a\cdot p(T_c-T_5)+\frac{\lambda_2\cdot a\cdot p}{d/20}(T_4-T_5)+\varepsilon\cdot\sigma\cdot a\cdot p(T_6^2+T_5^2)(T_6+T_5)(T_6-T_5)=$$

$$\rho\cdot a\cdot(d/20)\cdot p\cdot C_{p,elec}\frac{\partial T_5}{\partial t}$$

- Middle cathode temperature (T_c):

$$h_{C,elec}\cdot a\cdot p(T_5-T_c)+h_{C,I}\cdot a\cdot p(T_6-T_c)+\dot{m}_C\cdot c_{p,Air}(T_{Cin}-T_c)+\dot{m}_C\cdot c_{p,Air}(T_{Cout}-T_c)=\rho\cdot a\cdot e\cdot p\cdot C_{p,C}\frac{\partial T_c}{\partial t}$$

- Temperature between cathode interconnect and cathode (T_6):

$$\frac{\lambda_1\cdot a\cdot p}{b/2}(T_{Ic}-T_6)+h_{C,I}\cdot a\cdot p(T_c-T_6)+\varepsilon\cdot\sigma\cdot a\cdot p(T_5^2+T_6^2)(T_5+T_6)(T_5-T_6)=$$

$$\rho\cdot a\cdot b/4\cdot p\cdot C_{p,I}\frac{\partial T_6}{\partial t}$$

- Middle cathode interconnect temperature (T_{Ic}):

$$\frac{\lambda_1 \cdot a \cdot p}{b/2}(T_{sc} - T_{Ic}) + \frac{\lambda_1 \cdot a \cdot p}{b/2}(T_6 - T_{Ic}) = \rho \cdot a \cdot b/2 \cdot p \cdot C_{p,I} \frac{\partial T_{Ic}}{\partial t}$$

- Temperature between cathode interconnect and furnace (T_{sc}):

$$h_{I,amb} \cdot a \cdot p(T_{ext} - T_{sc}) + \varepsilon \cdot \sigma \cdot a \cdot p(T_{ext}^2 + T_{sc}^2)(T_{ext} + T_{sc})(T_{ext} - T_{sc}) + \frac{\lambda_1 \cdot a \cdot p}{b/2}(T_{Ic} - T_{sc}) =$$

$$\rho \cdot a \cdot b/4 \cdot p \cdot C_{p,I} \frac{\partial T_{sc}}{\partial t}$$